17th Brazilian Congress of Thermal Sciences and Engineering
November 25th-28th, 2018, Águas de Lindóia, SP, Brazil

ENCIT-2018-0164

COMPARISON OF DIFFERENT TECHNIQUES TO SPECIFY BOUNDARY CONDITIONS IN BODY-FITTED GRIDS

Aline Roberta Santos Righi
Luciano Kiyoshi Araki
Federal University of Paraná
Block IV - Polytechnique Center – Jardim das Américas – Curitiba – Brazil
alinerighi29@gmail.com, lucaraki@ufpr.br

Abstract.*All CFD problems are defined in terms of initial and boundary conditions: a misleading in correctly specifying boundary conditions conducts to inaccurate numerical solutions. Based on this, the main purpose of this work is to compare different techniques available in literature to specify boundary conditions in body-fitted grids for a Poisson-type problem.*

Keywords:*body-fitted grids, boundary conditions, Lagrange interpolation, elliptical differencing interpolation*

1. INTRODUCTION

Among all methods applicable to the study of problems in Computational Fluid Dynamics (CFD) and Computational Heat Transfer (CHT), one of the most widely used is the Finite-Volume Method (FVM) (Juretic and Gosman, 2010). An essential advantage of the FVM is connected to the very important concept of conservative discretization; the FVM is also perfectly adapted to arbitrary grids (Hirsch, 2007), which is very important in real engineering problems.

Many problems of interest in heat transfer and fluid flows are defined in irregular geometries, such as furnaces, modern pent-roof combustion chambers in internal combustion engines, intake and exhaust ports and flow passages, turbomachinery and many more. CFD methods for complex geometries are classified in two groups: (i) structured curvilinear grid arrangements and (ii) unstructured grid arrangements (Versteeg and Malalasekera, 2007).

Structured curvilinear grids or body-fitted grids are based on mapping of the flow/heat transfer domain onto a computational domain with a simple shape (Versteeg and Malalasekera, 2007). The use of body-fitted grids is advantageous when compared to non-structured grids especially by the fact that the discretization processes provide diagonal matrices, which can be dealt by optimized solvers (Maliska, 2004).

All CFD problems are defined in terms of initial and boundary conditions: it is important that the user specifies these correctly and understands their role to the numerical algorithm (Versteeg and Malalasekera, 2007). There are three basic boundary condition types in literature: (i) Dirichlet, in which the unknown is defined at the boundaries; (ii) Neumann, in which the unknown derivative is specified at the boundaries; and (iii) Robin, in which a function mixing the unknown and its derivative is specified at the boundaries (Patankar, 1980; Weisstein, 2009).

In a sense the process of solving a field problem is nothing more than the extrapolation of a set of data defined on a boundary contour or surface into the domain interior. Because of this, it is of prior importance that boundary conditions are supplied in a realistic, well-posed form. Otherwise, severe difficulties are encountered in obtaining numerical solutions (Versteeg and Malalasekera, 2007).

Giacomini (2009) applied Dirichlet boundary conditions to 1D-CFD problems with uniform grids using four techniques: (i) ghost volumes; (ii) incorporating boundary conditions in volumes adjacent to the contour; (iii) using a null-width cell; and (iv) using half-volumes. According to the author, the used technique to apply the boundary condition can modify the convergence order of some variables of interest.

Based on all previously data, the main proposal of this work is to provide numerical analyses mixing both body-fitted grids and the application of boundary conditions by different techniques. The mathematical model, presented in Section 2, consists of a Poisson-type equation, which is discretized using the coordinate transformation as described by Maliska (2004). Numerical results are provided in Section 4, while the final remarks are presented in Section 5.

2. METHODOLOGY

2.1 Mathematical model

Poisson-type equations can be used to model heat diffusion problems as well as some fluid flow problems in stream function formulation (Kundu and Cohen, 2008). Such equation, in Cartesian coordinate system, is expressed as

$$\frac{\partial^2 T}{\partial x^2} + \frac{\partial^2 T}{\partial y^2} = S \tag{1}$$

where: T is the temperature, x and y are the coordinate directions and S is the source term, which can be constant or not, depending on the phenomena it models. In this work, the source term S is taken as

$$S = -\frac{\pi^2}{2}\sin\left(\frac{\pi x}{2}\right)\sin\left(\frac{\pi y}{2}\right) \tag{2}$$

which was obtained in order to provide an analytical solution to the temperature field over all domain by the method of manufactured solutions (Salari and Knupp, 2000). In this case, whatever be the domain, analytical solution is given by

$$T(x,y) = \sin\left(\frac{\pi x}{2}\right)\sin\left(\frac{\pi y}{2}\right) \tag{3}$$

Boundary conditions of any type (Dirichlet, Neumann or Robin) can be obtained by using Eq. (3).

Two different geometries are used in order to compare numerical results: a L-shaped one and a trapezoidal one (Figure 1). In addition, boundary conditions are obtained by the analytical solution (Eq. (3)), and for the L-shaped are given by

$$T(x,0) = T(0,x) = 0 \tag{4}$$

$$T(x,1) = \sin\left(\frac{\pi x}{2}\right), \text{ if } 0 \le x \le \frac{1}{2} \tag{5}$$

$$T\left(x,\frac{1}{2}\right) = \frac{\sqrt{2}}{2}\sin\left(\frac{\pi x}{2}\right), \text{ if } \frac{1}{2} \le x \le 1 \tag{6}$$

$$T(1,y) = \sin\left(\frac{\pi y}{2}\right), \text{ if } 0 \le y \le \frac{1}{2} \tag{7}$$

$$T\left(\frac{1}{2},y\right) = \frac{\sqrt{2}}{2}\sin\left(\frac{\pi y}{2}\right), \text{ if } \frac{1}{2} \le y \le 1 \tag{8}$$

also, for the trapezoidal, boundary conditions are given by Eqs. (6) and (7)

$$T(x,y) = \sin\left(\frac{\pi x}{2}\right)\sin\left(\frac{\pi y}{2}\right), \text{ if } 0 \le x \le \frac{1}{2} \text{ and } 0 \le y \le \frac{1}{2} \tag{9}$$

2.2 Numerical models

In order to work with body-fitted grids, the Cartesian coordinate system, the physical plan, is transformed into the computational plan, where $(x,y) \to (\xi,\eta)$ for a 2D system (Figure 2). Maliska (2004) describes the transformation for a generic equation of conservation. Being $f = f(\xi,\eta)$ where f is the independent variable, the derivatives through the chain rule are

$$\frac{\partial f}{\partial x} = \frac{\partial f}{\partial \xi}\frac{\partial \xi}{\partial x} + \frac{\partial f}{\partial \eta}\frac{\partial \eta}{\partial x} \tag{10}$$

$$\frac{\partial f}{\partial y} = \frac{\partial f}{\partial \xi}\frac{\partial \xi}{\partial y} + \frac{\partial f}{\partial \eta}\frac{\partial \eta}{\partial y} \tag{11}$$

If $f = x$ applied in Eq. (10) and $f = y$ for Eq. (11), the solution is

$$\xi_x = y_\eta \; J \tag{12}$$

$$\eta_x = - y_\xi \; J \tag{13}$$

where J is the Jacobian of the transformation, and is given by

$$J = (x_\xi \, y_\eta + x_\eta \, y_\xi)^{(-1)} \tag{14}$$

Later, applying $f = x$ in Eq. (11) and $f = y$ for Eq. (10)

$$\xi_y = - x_\eta \; J \tag{15}$$

$$\eta_y = x_\xi \; J \tag{16}$$

and J is the Jacobian represented by Eq.(14). Given that, Eqs. (12), (13), (15) and (16) are the transformation metrics, which jointly with the Jacobian will appear in the transformed equation.

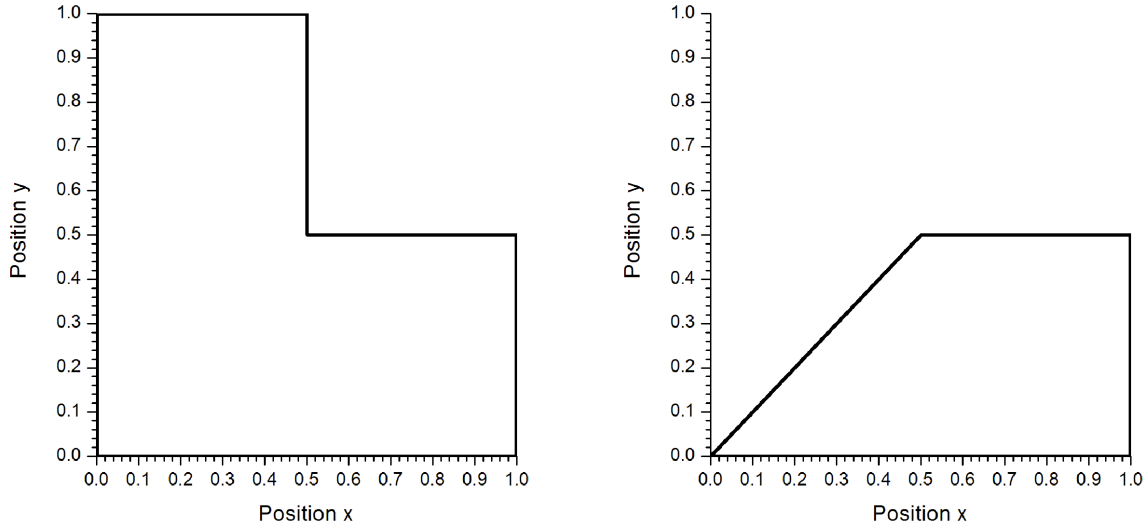

(a) (b)

Figure 1. Geometries used to solve the Poisson-type equation: (a) L-shape; (b) trapezoidal.

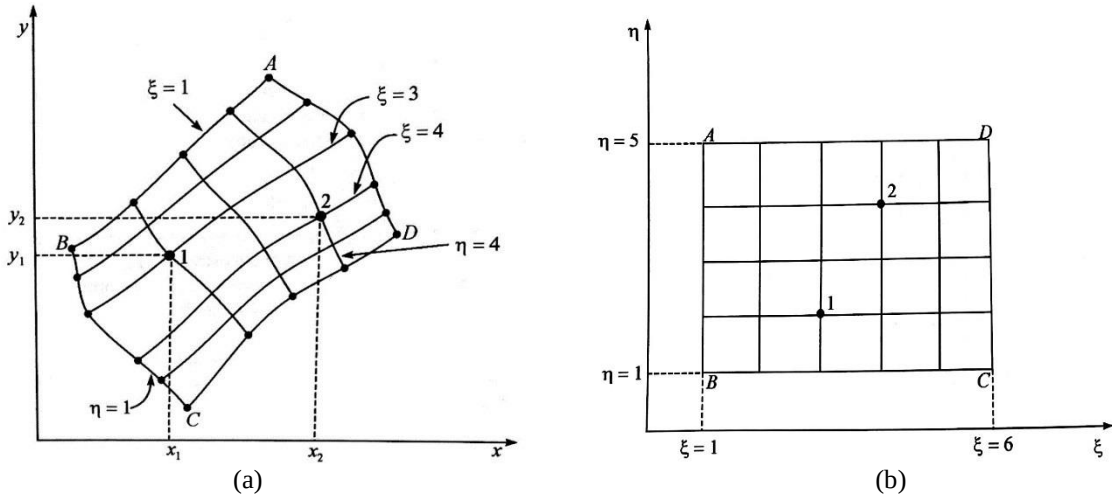

(a) (b)

Figure 2. (a) Physical plan; (b) Computational plan (Adapted from Maliska, 2004).

Moreover, according to Maliska (2004), the areas of a 2D curvilinear coordinate can be obtained by the expressions

$$d\,L_\xi = \sqrt{\gamma}\;\Delta\xi \tag{17}$$

$$d\,L_\eta = \sqrt{\alpha}\;\Delta\eta \tag{18}$$

where $d\,L_\xi$ and $d\,L_\eta$ are the length along the axis ξ and η; and $\gamma = \left(y_\xi^2 + x_\xi^2\right)$ and $\alpha = \left(y_\eta^2 + x_\eta^2\right)$ are obtained by the Pythagorean Theorem. This way, the area given by Eq. (17) and Eq. (18) is

$$dA = \left(x_\xi\, y_\eta - x_\eta\, y_\xi\right)\Delta\xi\;\Delta\eta \tag{19}$$

which, remembering that $J = (x_\xi\, y_\eta + x_\eta\, y_\xi)^{(-1)}$, gives an important interpretation since it is possible to conclude that the relation between the areas of the physical and transformed plan is $1/J$ (Maliska, 2004). Therefore, through the determinant of the metric tensor

$$\beta = x_\xi\, x_\eta + y_\xi\, y_\eta \tag{20}$$

where β represents the non-orthogonality of the curvilinear coordinate, and it is also represented by $\beta = \sqrt{\alpha\gamma}\,\cos\theta$.

Given that, equation (1) is then transformed to a $\xi - \eta$ system of coordinates providing

$$\frac{\partial}{\partial\xi}\left[J\left(\alpha\frac{\partial T}{\partial\xi} - \beta\frac{\partial T}{\partial\eta}\right)\right] + \frac{\partial}{\partial\eta}\left[J\left(\gamma\frac{\partial T}{\partial\eta} - \beta\frac{\partial T}{\partial\xi}\right)\right] = \frac{S}{J} \tag{21}$$

where *J* is the determinant of the Jacobian matrix given by Eq.(14); and α, β and γ are the transformation metrics.

The discretization of Eq. (21) is done by using the Finite Volume Method (Maliska, 2004; Versteeg and Malalasekera, 2007), with non-starred grids and second order Central Differencing Scheme (CDS-2), providing the system of linear equations in the form:

$$a_P T_P = a_W T_W + a_E T_E + a_S T_S + a_N T_N + a_{SW} T_{SW} + a_{SE} T_{SE} + a_{NW} T_{NW} + a_{NE} T_{NE} + b_P \tag{22}$$

where:

$$a_W = J_w\alpha_w\frac{\Delta\eta}{\Delta\xi} + \frac{1}{4}J_n\beta_n - \frac{1}{4}J_s\beta_s; \qquad a_E = J_e\alpha_e\frac{\Delta\eta}{\Delta\xi} - \frac{1}{4}J_n\beta_n + \frac{1}{4}J_s\beta_s \tag{23}$$

$$a_S = J_s\gamma_s\frac{\Delta\xi}{\Delta\eta} + \frac{1}{4}J_e\beta_e - \frac{1}{4}J_w\beta_w; \qquad a_N = J_n\gamma_n\frac{\Delta\xi}{\Delta\eta} - \frac{1}{4}J_e\beta_e + \frac{1}{4}J_w\beta_w \tag{24}$$

$$a_{SW} = -\frac{1}{4}J_w\beta_w - \frac{1}{4}J_s\beta_s; \qquad a_{SE} = \frac{1}{4}J_e\beta_e + \frac{1}{4}J_s\beta_s \tag{25}$$

$$a_{NW} = \frac{1}{4}J_w\beta_w + \frac{1}{4}J_n\beta_n; \qquad a_{NE} = -\frac{1}{4}J_e\beta_e - \frac{1}{4}J_n\beta_n \tag{26}$$

$$a_P = a_W + a_E + a_S + a_N + a_{SW} + a_{SE} + a_{NW} + a_{NE} \tag{27}$$

$$b_P = -S_P\frac{\Delta\xi\,\Delta\eta}{J_P} \tag{28}$$

which are valid for all internal volumes, and such system of equations can be solved by a 9-diagonal Gauss-Seidel method. Since the coordinate transformation is valid for any domain geometry, Eqs.(23) to (28) are valid for both geometries. For both geometries, two discretization procedures were employed: (i) consisting on line segments obtained by Lagrange interpolation; and (ii) consisting on lines obtained by solving elliptical differencing equations. Both procedures are presented by Maliska (2004) and Figs. 3a and 3b, also Figs. 4a and 4b bring examples.

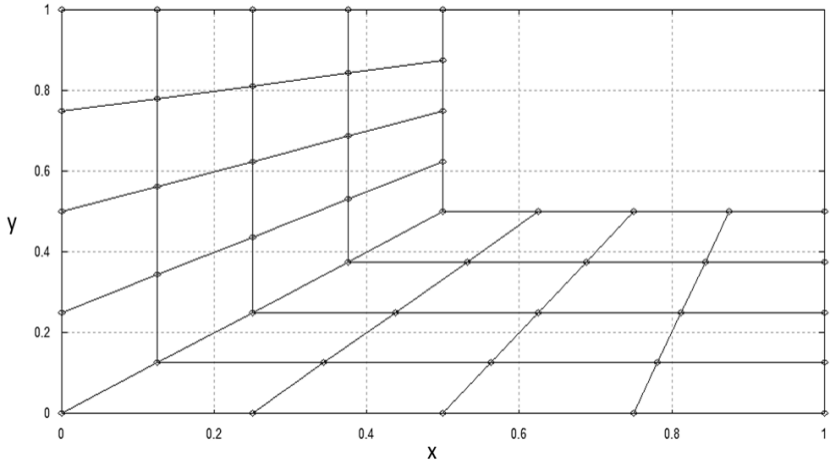

Figure 3a. L-shape with the Lagrange interporlation.

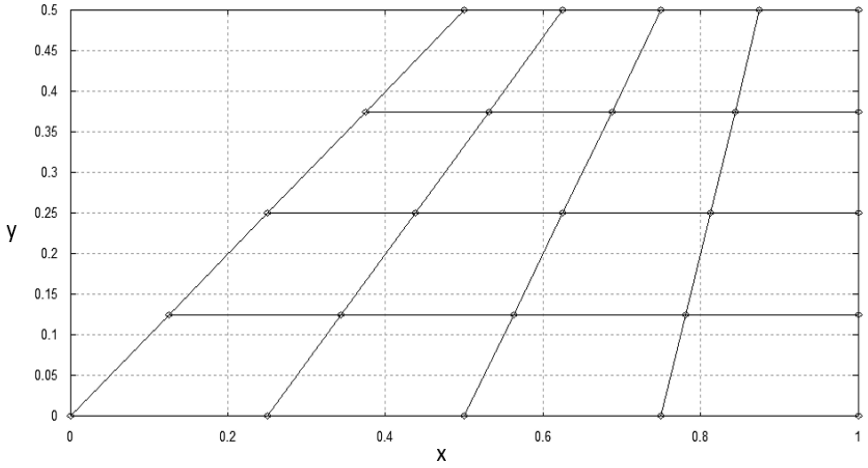

Figure 3b. Trapezoidal for the Lagrange interpolation.

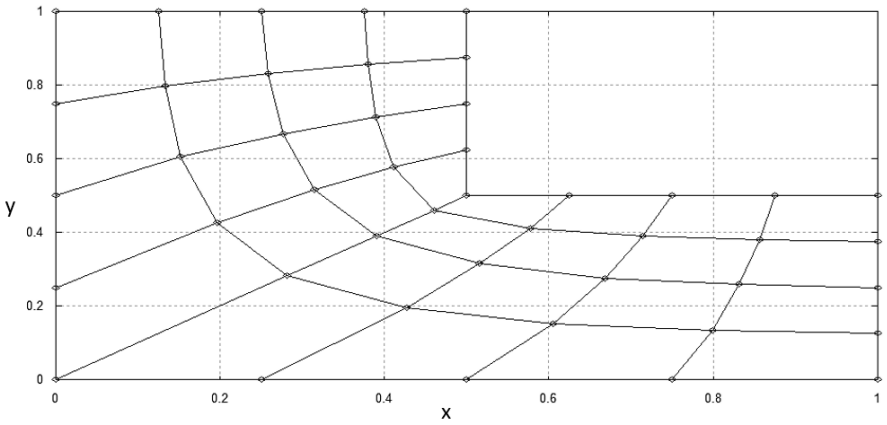

Figure 4a. L-shape with the elliptical differencing equations.

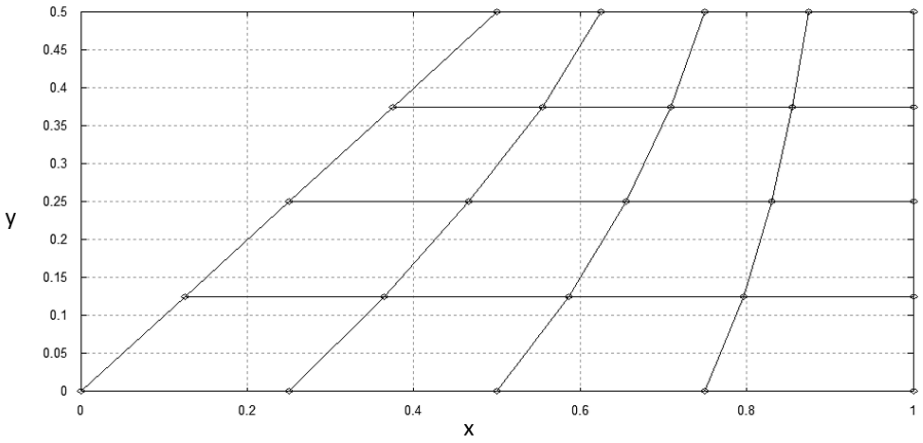

Figure 4b. Trapezoidal with the elliptical differencing equations.

2.3 Boundary conditions

Boundary conditions, firstly considered as Dirichlet ones, are applied by using the technique of ghost-cells, which were previously employed by Giacomini (2009) to 1D-CFD problems. The technique of ghost-cells consists in adding one more volume in the boundaries, which are not part of the main domain. Given that, Fig. (5), for example, represents an east and west sides, and the same form is applied for the north and south boundaries.

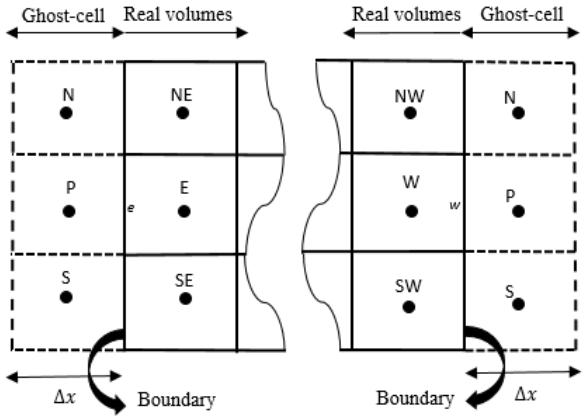

Figure 5. Technique of ghost-cells for boundary conditions.

Applying the technique in the boundaries, the coefficients provided for the east side are

$$a_P = 1; \quad a_W = -1; \quad b_P = 2Tw \tag{29}$$

where the others coefficients are zero, T_w is the are prescribed temperature and can be evaluated by Eq. (7). The same is done for the others contours, and coefficients (29) are valid for both geometries.

Later, applying ghost-cells for boundary conditions as Neumann ones, the coefficients for the east side are

$$a_P = 1; \quad a_W = 1; \tag{30}$$

$$a_N = a_{NW} = \frac{\Delta\xi}{4\Delta\eta}\frac{\beta_w}{\alpha_w} \tag{31}$$

$$a_S = a_{SW} = -\frac{\Delta\xi}{4\Delta\eta}\frac{\beta_w}{\alpha_w} \tag{32}$$

$$b_P = \frac{q''}{\Gamma^{\phi}} \frac{\Delta\xi}{J_W \alpha^{1/2}} \tag{33}$$

where J_W is the Jacobian; and q''/Γ^{ϕ} is the flux and it can be evaluated by the derivative of the boundary condition correspondent to the contour. Coefficients (30) to (33) are valid for both geometries, and the same is applied for one more contour, which one that can be convenient. However, as it can be seen, boundary conditions as Neumann ones are applied for only two boundaries of the domain, because if applying for all boundaries it is possible to obtain infinity solutions.

3. NUMERICAL VERIFICATION AND POST-PROCESSING

In order to verify the convergence order of the solution, different grids were used, starting with a coarse grid until a fine one. Numerical analysis of results consists on determination of apparent (p_U) and effective (p_E) convergence orders (Marchi, 2001; Marchi and Silva, 2005), which are evaluated by

$$p_U = \frac{\log\left(\frac{\phi_2 - \phi_1}{\phi_3 - \phi_2}\right)}{\log(q)}, \qquad p_E = \frac{\log\left(\frac{E(\phi_2)}{E(\phi_1)}\right)}{\log(q)} \tag{34}$$

where: ϕ is the numerical solution; q is the refinement ratio; indices 1, 2 and 3 are related to a coarse, intermediate and fine grids; and $E(\phi)$ is the numerical error, defined as the difference between the analytical value of the property ϕ and its numerical solution. According to Marchi (2001), both apparent and effective order allow in the post-processing the verification if the uncertain order of the numerical solution tends to the asymptotic order while the grid is refined.

The numerical analysis are made from the solutions for the average temperature based on the rectangle rule, expressed as

$$\overline{T_{2D}} \approx \frac{1}{A} \sum_P T_P \, \Delta A_P \tag{35}$$

where $\Delta A_P = \Delta\xi \, \Delta\eta / |J_P|$ and $A = \Delta\xi \, \Delta\eta \sum_P \left(\frac{1}{J_P}\right)$.

4. NUMERICAL RESULTS

First studies include the use of ghost-cells to specify Dirichlet boundary conditions. As can be seen in Figs. 6 and 7, for all cases both apparent and effective convergence orders do not have the tendency to the asymptotic value of 2.

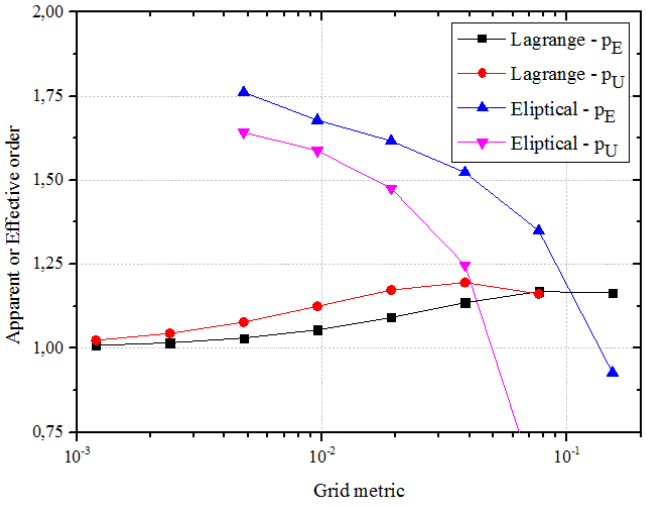

Figure 6. Apparent and effective orders for the L-shape geometry with Dirichlet boundary conditions.

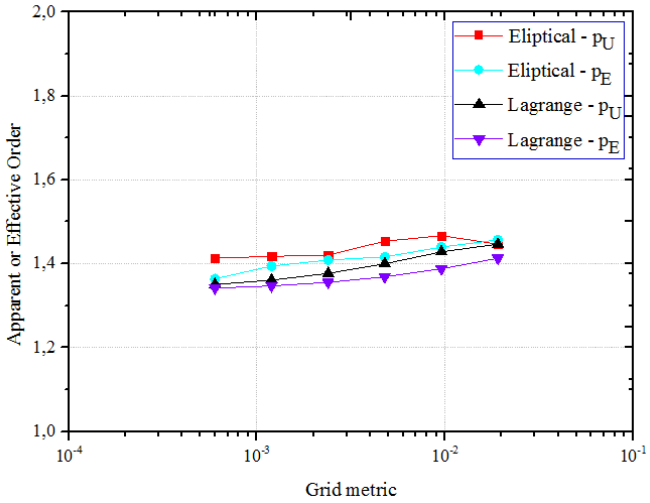

Figure 7. Apparent and effective orders for the trapezoidal geometry with Dirichlet boundary conditions.

Furthermore, for all cases the numerical error is shown in Figs. (8) and (9), and as it can be seen, the numerical error is smaller as the grid metric tends to zero. In addition, a second study includes the technique of ghost-cells for Neumann boundary conditions applied for both geometries. The coefficients were applied for the west and east boundaries, which ones were chosen for analysis of the convergence orders. Figures 10 and 11 show the apparent and effective order for all cases, and as it can be seen, the convergences orders do not have the tendency of the asymptotic order, 2.

The numerical error of the solution for all cases are shown in Figs. 12 and 13, and it can be observed that even though for all cases the error is smaller as the grid tends to zero, for the L-shape the solution converges to a better number than that for the trapezoidal shape. Such behavior occurs for both Dirichlet and Neumann boundary conditions.

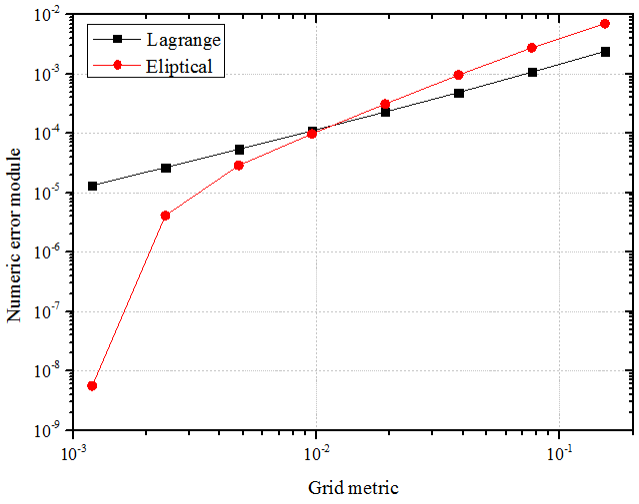

Figure 8. Numerical error module for the L-shape geometry with Dirichlet boundary conditions.

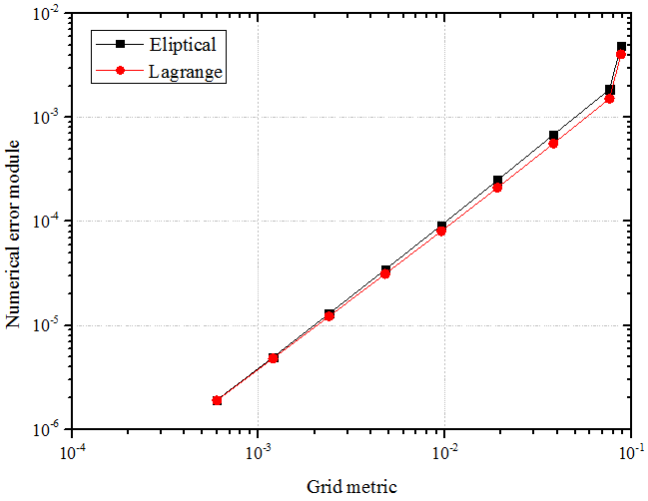

Figure 9. Numerical error module for the trapezoidal geometry with Dirichlet boundary conditions.

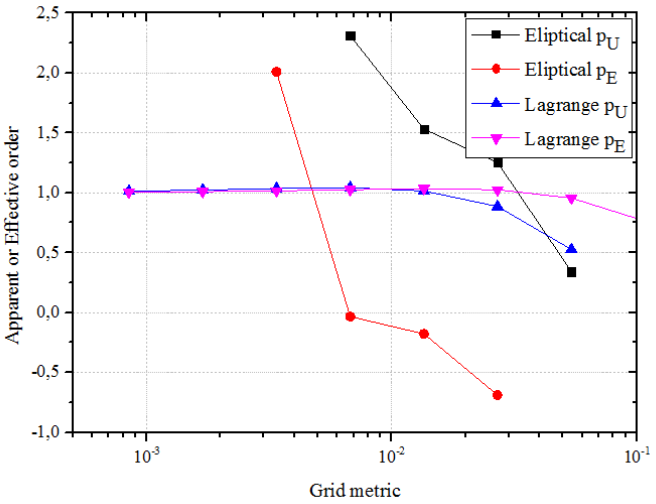

Figure 10. Apparent and effective orders for the L-shape geometry with Neumann boundary conditions.

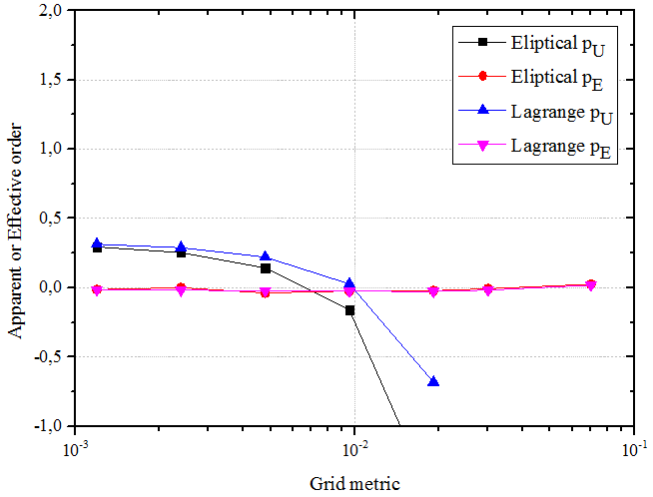

Figure 11. Apparent and effective orders for the trapezoidal geometry with Neumann boundary conditions.

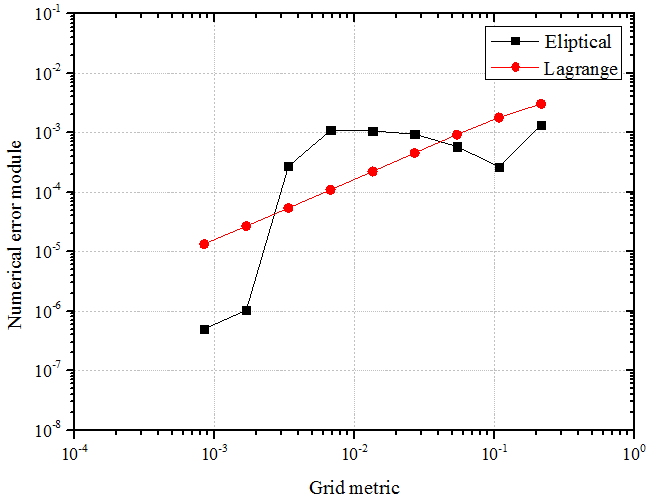

Figure 12. Numerical error module for the L-shape geometry with Neumann boundary conditions.

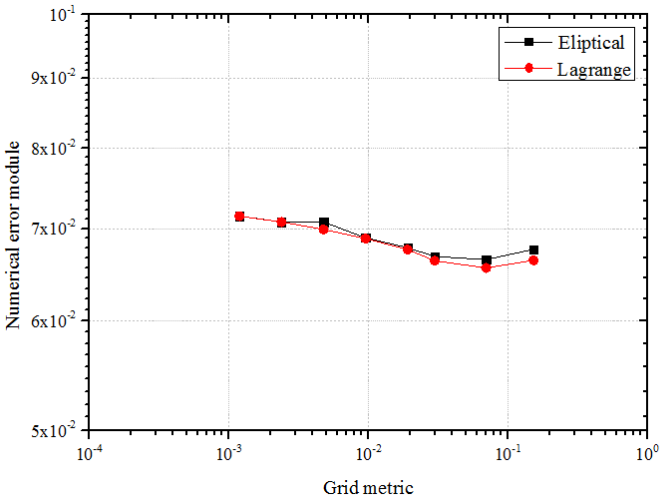

Figure 13. Numerical error module for the trapezoidal geometry with Neumann boundary conditions.

5. CONCLUSION

Firstly, the main purpose was to find the method with the best convergence order, since it is unexpected that the effective and apparent orders do not have the tendency of the asymptotic order, which has a value of two. In addition, according to Maliska (2004), in engineering problems, the most important part is to correctly choose and apply the boundary conditions, considering that a bad choice can compromise the entire solution. Given that, the struggle was to find the best numerical solution when the grid metric tends to zero, and at the same time, the best convergence order.

In conclusion, for all cases the solution of the numerical average temperature tends to the analytical average temperature when the grid metric tends to zero. However, for the L-shape geometry the solution of the numerical error shows a better convergence when compared to the trapezoidal geometry. Moreover, when it comes to the effective and apparent order, the elliptical differencing equations shows a better solution than the Lagrange interpolations. Even more, the orders have shown a better number for the L-shape geometry for all cases than for the trapezoidal geometry. Table 1 summarize the numbers found for the convergences in all cases studied.

Even though the convergence order is not what was expected, Ferziger and Perić (2002) points out some of the difficult find when working with non-orthogonal mesh. For example, considering the transformed equation (21), the derivatives are multiplied by the β that represents the non-orthogonality of the grid and depends on the angles between the grid lines and on the grid aspect radio. In this way, if the angle between the grid lines is small and the aspect radio is large, this can lead to poor convergence and oscillations in the solution. Finally, when working applying Neumann boundary conditions, the discretization process can influence in the orders.

Table 1. Values for the orders achieved in all cases studied.

Boundary condition / Domain / Grid generation	Assymptotic	Effective	Apparent
Dirichlet L-shape Lagrange	2.00	1.00	1.02
Dirichlet L-shape Elliptical	2.00	1.76	1.64
Dirichlet Trapezoidal Lagrange	2.00	1.34	1.35
Dirichlet Trapezoidal Elliptical	2.00	1.36	1.41
Neumann L-shape Lagrange	2.00	1.00	1.01
Neumann L-shape Elliptical	2.00	2.00	2.31
Neumman Trapezoidal Lagrange	2.00	0.01	0.32
Neumman Trapezoidal Elliptical	2.00	0.01	0.31

6. ACKNOWLEDGEMENTS

The authors would acknowledge Federal University of Paraná (UFPR), Coordenação de Aperfeiçoamento de Pessoal de Nível Superior (CAPES) and Conselho Nacional de Desenvolvimento Científico e Tecnológico (CNPq) by physical and financial support given for this work.

7. REFERENCES

Ferziger, J. H., Perić, M., 2002, *Computational Methods for Fluid Dynamics.* Springer, Germany, 3nd edition.

Giacomini, F.F., 2009, *Verificação da Forma de Aplicar Condições de Contorno em Problemas Unidimensionais com o Método dos Volumes Finitos*, Master Thesis, Federal University of Paraná, Curitiba.

Hirsch, C. *Numerical Computation of Internal & External Flows – Volume 1: Fundamentals of Computational Fluid Dynamics*. Butterworth-Heinemann, Oxford, 2nd edition.

Juretic, F. and Gosman, A.D., 2010, "Error Analysis of the Finite-Volume Method with Respect to Mesh Type". *Numerical Heat Transfer, Part B*, Vol. 57, p. 410-439.

Kundu, P.K and Cohen, I.M., 2008, *Fluid Mechanics*. Academic Press, Burlington, 4th edition.

Maliska, C.R., 2004. *Transferência de Calor e Mecânica dos Fluidos Computacional*. LTC Editora, Rio de Janeiro, 2nd edition.

Marchi, C.H., 2001, *Verificação de Soluções Numéricas Unidimensionais em Dinâmica dos Fluidos*, PhD Thesis, Federal University of Santa Catarina, Florianópolis.

Marchi, C.H., Silva, A.F.C., 2005, "Multi-dimensional Discretization Error Estimation for Convergent Apparent Order", *Journal of the Brazilian Society of Mechanical Sciences and Engineering*, Vol. 27, p. 432-439.

Patankar, S.V., 1980 *Numerical Heat Transfer and Fluid Flow*. Taylor and Francis: New York.

Salari, K. and Knupp, P., 2000, "Code Verification by the Method of Manufactured Solutions". *Sandia Report SAND2000-1444.*

Versteeg, H.K. and Malalasekera, W., 2007, *An Introduction to Computational Fluid Dynamics – The Finite Volume Method*. Pearson Education Limited, Harlow, 2nd edition.

8. RESPONSIBILITY NOTICE

The authors are the only responsible for the printed material included in this paper.